Plant Physiology Preview. Published on September 2, 2014, as DOI:10.1104/pp.114.244319

Voltage-sensor transitions of the inward-rectifying K^+ channel KAT1 indicate a latching mechanism biased by hydration within the voltage sensor

Cécile Lefoulon, Rucha Karnik, Annegret Honsbein, Paul Vijay Gutla, Christopher Grefen[1], Janin Riedelsberger[2,3], Tomás Poblete[2], Ingo Dreyer[3,4], Wendy Gonzalez[2,3,5], and Michael R. Blatt[6]

Laboratory of Plant Physiology and Biophysics, Bower Building, University of Glasgow, Glasgow G12 8QQ UK

[1]Current address: ZMBP Developmental Genetics, Auf der Morgenstelle 1, D72076 Tuebingen Germany

[2]Centro de Bioinformatica y Simulacion Molecular, Universidad de Talca, Casilla 721, Talca, Chile

[3]University of Potsdam, Biochemistry and Biology Group BPMBP, Karl-Liebknecht-Strasse 24-25, Haus 20, D14476 Golm, Germany

[4]Centre for Biotechnology and Plant Genomics UPM, INIA, 28223 Pozuelo de Alacon, Madrid, Spain

[5]Author for correspondence relating to channel modelling (wgonzalez@utalca.cl)

[6]Corresponding author: M.R. Blatt (email michael.blatt@glasgow.ac.uk)

Running Head: Dynamics of the KAT1 K^+ channel voltage sensor

Summary: Manipulating the electrostatic charge network that stabilizes the voltage sensor of the KAT1 K^+ channel displaces channel gating across more than 140 mV within the physiological voltage range.

ABSTRACT

The Kv-like K^+ channels at the plasma membrane, including the inward-rectifying KAT1 K^+ channel of Arabidopsis, are important targets for manipulating K^+ homeostasis in plants. Gating modification, especially, has been identified as a promising means by which to engineer plants with improved characteristics in mineral and water use. Understanding plant K^+ channel gating poses several challenges, despite many similarities to that of mammalian Kv and Shaker channel models. We have used site-mutagenesis to explore residues that are thought to form two electrostatic counter-charge centers either side of a conserved Phe residue within the S2 and S3 α-helices of the voltage sensor domain (VSD) of Kv channels. Consistent with molecular dynamic simulations of KAT1, we show that the voltage dependence of the channel gate is highly sensitive to manipulations affecting these residues. Mutations of the central Phe residue favored the closed KAT1 channel, whereas mutations affecting the counter-charge centers favored the open channel. Modelling of the macroscopic current kinetics also highlighted a substantial difference between the two sets of mutations. We interpret these findings in context of the effects on hydration of amino-acid residues within the VSD and with an inherent bias of the VSD, when hydrated around a central Phe residue, to the closed state of the channel.

Keywords: K^+ channel, voltage-dependent / voltage-sensor domain / KAT1 gating conformation / electrostatic charge-charge compensation / plant K^+ channel / Arabidopsis

INTRODUCTION

Plant cells utilise the potassium ion (K^+) to maintain hydrostatic (turgor) pressure, to drive irreversible cell expansion for growth, and to facilitate reversible changes in cell volume during stomatal movements. Potassium uptake and its circulation throughout the plant relies both on high-affinity, H^+-coupled K^+ transport (Quintero and Blatt 1997; Rubio et al. 2008) and on K^+ channels to facilitate K^+ ion transfer across cell membranes. Uptake via K^+ channels is thought to be responsible for roughly 50% of the total K^+ content of the plant under most field conditions (Spalding et al. 1999; Rubio et al. 2008; Amtmann and Blatt 2009). K^+ channels confer on the membranes of virtually every tissue distinct K^+ conductances and regulatory characteristics (Very and Sentenac 2003; Dreyer and Blatt 2009). Their characteristics are thus of interest for engineering directed to manipulating K^+ flux in many aspects of plant growth and cellular homeostasis. The control of K^+ channel gating has been identified as the most promising target for genetic engineering of stomatal responsiveness (Lawson and Blatt 2014; Wang et al. 2014a), based on the recent developments of quantitative systems models of guard cell transport and metabolism (Wang et al. 2012; Hills et al. 2012; Chen et al. 2012b). By contrast, modifying expression and, most likely, the population of native K^+ channels at the membrane was found to have no substantial effect on stomatal physiology (Wang et al. 2014b).

The Kv-like K^+ channels of the plant plasma membrane (Pilot et al. 2003; Dreyer and Blatt 2009) share a number of structural features with the Kv superfamily of K^+ channels characterized in animals and *Drosophila melanogaster* (Papazian et al. 1987; Pongs et al. 1988). The functional channels assemble from four homologous subunits and surround a central, transmembrane pore that forms the permeation pathway (Daram et al. 1997). Each subunit comprises six transmembrane α-helices, designated S1-S6, and both N- and C-termini are situated on the cytosolic side of the membrane (Uozumi et al. 1998). The pore or P loop between the S5 and S6 α-helices incorporates a short α-helical stretch and the highly-conserved amino-acid sequence TxGYGD, which forms a selectivity filter for K^+ (Uozumi et al. 1995; Becker et al. 1996; Nakamura et al. 1997). The carbonyl oxygen atoms of these residues in all four K^+ channel subunits face inward to form coordination sites for K^+ ions between them (Doyle et al. 1998; Jiang et al. 2003; Kuo et al. 2003; Long et al. 2005) and a multi-ion pore (Thiel and Blatt 1991) such that K^+ ions pass through the selectivity

filter as if in free solution. The plant channels are also sensitive to a class of neurotoxins that exhibit high specificity in binding around the mouth of the channel pore (Obermeyer et al. 1994).

These K^+ channels also share a common gating mechanism. Within each subunit, the first four α-helices form a quasi-independent unit, the voltage sensor domain (VSD), with the S4 α-helix incorporating positively charged (Arg or Lys) residues regularly positioned across the lipid bilayer and transmembrane electric field. Voltage displaces the S4 α-helix within the membrane and couples rotation of the, S5 and S6 α-helices lining the pore, thereby opening or closing the channel (Sigworth 2003; Dreyer and Blatt 2009). For outward-rectifying channels, such as the mammalian Kv1.2 and *Drosophila Shaker* K^+ channels, an inside-positive electric field drives the positively-charged, S4 α-helix outward (the 'up' position) which draws on the S4-S5 linker to open the pore. This simple expedient of a 'lever and string' secures current flow in one direction by favouring opening at positive, but not negative voltages. This same model applies to the Arabidopsis Kv-like K^+ channels, including outward-rectifiers that exhibit sensitivity to external K^+ concentration (Blatt 1988; Blatt and Gradmann 1997; Johansson et al. 2006), and it serves equally in the gating of inward-rectifying K^+ channels such as KAT1 which gates open at negative voltages (Dreyer and Blatt 2009).

Studies of KAT1 gating (Latorre et al. 2003; Lai et al. 2005) have indicated that the S4 α-helix of the channel most likely undergoes very similar conformational changes with voltage as those of the mammalian and *Shaker* K^+ channels. These findings conform with the present understanding of the evolution of VSD structure (Palovcak et al. 2014) and the view of a common functional dynamic to its molecular design. It is likely, therefore, that a similar electrostatic network occurs in KAT1 to stabilize the VSD. Crucially, however, experimental evidence in support of such a network has yet to surface. Electrostatic counter-charges and hydration of amino-acid side chains between the α-helices within the VSDs of mammalian and *Shaker* K^+ channel models are important for the latch-like stabilization of the 'down' and 'up' states of these channels (Tao et al. 2010; Pless et al. 2011). Nonetheless, several studies (Gajdanowicz et al. 2009; Riedelsberger et al. 2010) have pointed to subtle differences in the structure of KAT1 that relate to the VSD.

We have explored the electrostatic network of the KAT1 VSD through site-directed mutagenesis to manipulate the voltage-dependence of the KAT1, combining these studies with with molecular dynamic simulations previously shown to accommodate the plant VSDs and their hydration during gating transitions (Gajdanowicz et al. 2009; Garcia-Mata et al. 2010). We report here that gating of KAT1 is sensitive to manipulations affecting a set of electrostatic charge transfer centers. The findings conform in large measure to the mammalian and *Shaker* models. However, virtually all manipulations affecting a highly-conserved, central Phe favor the 'up' state of the VSD and closed KAT1 channel, whereas mutations affecting the electrostatic networks either side of this Phe favor the 'down' state of the VSD and the open channel. These, and additional observations suggest that hydration within the VSD is a major determinant of KAT1 gating.

RESULTS

Substitutions of Phe^{102} in the S2 α-helix displace KAT1 channel opening to negative voltages

The S2 α-helix of the mammalian Kv and *Shaker* K^+ channels incorporates highly-conserved Glu or Asp and Phe residues that align with the corresponding amino acids in KAT1 as well as in other plant Kv-like K^+ channels (Fig. 1). Phe^{290} of the *Shaker* and Phe^{233} of the Kv1.2 K^+ channels situate roughly mid-way across the membrane. It is thought to present a hydrophobic barrier that separates a set of inner and outer pockets formed between the α-helices over which residues of the S4 must pass (Jensen et al. 2012); S4 charge movement is thought to be catalyzed relative to the other α-helices by means of the π electon cloud presented by the Phe (Pless et al. 2011). Substitutions at this site with aromatic amino acids have been reported to favor the S4 α-helix extended outward, the 'up' position (Pless et al. 2011), which for these outward-rectifying channels corresponds to the open channel. With Trp at this position, a Kv1.2-Kv2.1 VSD chimera (PDB 2R9R) is stabilized in the up conformation even at voltages negative of -50 mV, whereas substitutions with non-aromatic residues – including Asn, Thr, Ser and Leu – have been reported give mid-point voltages for half-maximal conductance ($V_{1/2}$) near and positive of 0 mV, thus favoring the 'down' position of the VSD when compared to the control (Tao et al. 2010).

We carried out the same subsitutions for Phe^{102} of KAT1 (Fig. 1) to test whether similar displacements in $V_{1/2}$ would be evident in the plant K^+ channel. When expressed in *Xenopus* oocytes, KAT1^{wt} normally yields a current with a $V_{1/2}$ near -140 mV and an apparent gating charge, δ, of -1.6 to -1.8 (Hoshi 1995; Zei and Aldrich 1998; Latorre et al. 2003; Gajdanowicz et al. 2009; Riedelsberger et al. 2010). As expected, we found the KAT1^{F102W} substitution to yield a channel that activated only near the negative voltage extreme that could be achieved with oocytes under voltage clamp (Fig. 2A,B). Substitution with Thr failed to give measurable currents. However, substitutions with each of the other non-aromatic amino acids also gave mutant KAT1 forms that activated variously at voltages negative of the wild-type K^+ channel. Joint fitting of these data sets with a Boltzmann function yielded good fits with gating charge and conductance maximum held in common between data sets, and with values for $V_{1/2}$ that in every case were displaced to voltages negative of KAT1^{wt} (Fig. 2A, Table 1).

We examined the effects of Phe^{102} substitutions on the kinetics of activation and deactivation of the KAT1 current. KAT1 activation is normally accelerated with voltages negative-going from -100 mV when stepped from a holding voltage of -50 mV and deactivates comparatively rapidly on steps back to voltages near and positive of -50 mV. To a first approximation, deactivation follows a simple exponential relaxation, but the current activates in sigmoid fashion (Hoshi 1995; Zei and Aldrich 1998), indicating two or more closed states of the channel. The current activates with halftimes of approximately 300 ms at -120 mV and with halftimes near 100 ms at -180 mV to -200 mV, while the current deactivates in roughly exponential fashion with time constants of 50 ms or less at -50 mV and more positive voltages, both in oocytes and in vivo (Eisenach et al. 2012; Chen et al. 2012a). We found that each of the mutations slowed KAT1 activation at any one voltage, the effect most pronounced with $KAT1^{F102W}$ and least with $KAT1^{F102L}$. The result was to displace activation halftimes as a function of voltage for each mutant negative-going from $KAT1^{wt}$ (Fig. 2C). Phe^{102} substitutions also accelerated current deactivation at -50 mV in roughly antiparallel fashion (Fig. 2D). These results therefore indicate that the substitutions have a substantial effect on the transitions between the open and closed states of the channel.

Simulations highlight an extended hydrophobic cavity that favors the 'down' state of the KAT1 VSD

It has been argued that this central Phe in the S2 α-helix forms a low-dielectric, hydrophobic barrier, isolating a water-filled pocket near the inner surface of the membrane (Tao et al. 2010; Lacroix et al. 2011). One challenge to questions of VSD conformation is that no crystal structure exists for the 'down' state, corresponding to the open KAT1 channel, which therefore cannot be inferred directly by homology modelling. To address this problem, structural models of KAT1, with the VSD in the 'up' and 'down' states, were built using as template the α-subunit of Kv1.2 that was derived *ab initio* with Rossetta (Yarov-Yarovoy et al. 2006). The 'down' state of this Kv1.2 model is compatible with experimental analysis of the KAT1 'down' state (Grabe et al. 2007) and indicates an open pore (Gajdanowicz et al. 2009) with the sequence alignment of Pathak, et al. (2007). Omitted from the homology mapping were residues Y^{114}-K^{126} of the extended S2-S3 cytoplasmic loop of KAT1 that is not present in the Kv1.2 sequence. Residues P^{148}-S^{160} between the S3 and S4 α-helices were

assigned to the external loop which, in Kv1.2, includes an additional eleven amino acids. Alignments and illustration of the KAT1 subunit structure, including the pore-lining α-helices for the homology model are included in Supplemental Fig. S1. This model for the KAT1 'down' state yielded a net 1.76 Å root mean squared difference (RMSD) across the entire VSD, demonstrating the accuracy of the fit to the Kv1.2 model; it reproduced the shallow angle of S4 α-helix and marked kink in the S3 α-helix, both present in the Kv1.2 model (Yarov-Yarovoy et al. 2006; Pathak et al. 2007); futhermore, it is the same model used successfully for KAT1 in past molecular dynamic simulations (Gajdanowicz et al. 2009; Riedelsberger et al. 2010). For simulations, the channel was equilibrated in the open and closed states (see Suppl. Fig. S2) before analysis of the water-filled space within the VSD and the atomic distances between the terminal residue carbons (CG for Asp, Glu and Asn, CZ for Arg, and CE for Lys). We report this C-C distance and the electrostatic and solvation energies in Table 2, calculated with an in-house script for the DESMOND program using the Schrödinger Python Suite 2012.

Initially, we examined Phe^{102} and its residue substitutions. Previous simulations (Gajdanowicz et al. 2009; Riedelsberger et al. 2010) indicated a substantial downward and rotational motion of the S4 relative to the S2 and S3 α-helices and movement of the positively-charged residues Arg^{171} and Arg^{174} across Phe^{102}. We analysed the radial distribution function (RDF) to determine the number of water molecules around residue 102 relative to free solution (Supplemental Fig. S3) and the hydrophobic vs. hydrophillic surface (Lins et al. 2003) accessible between the α-helices of the VSD. The latter is summarized in Fig. 3, which includes similar analysis for all of the other residue substitutions outlined in the following sections and discussed below. Significantly, both approaches predicted a substantial increase in hydration around residue position 102 in the Phe^{102} mutants when compared to $KAT1^{wt}$. The results were consistent with the idea that Phe^{102} forms a barrier for transition between closed and open states (Lacroix and Bezanilla 2011), in effect pointing to an occluded, hydrophobic pocket bounded by Phe^{102}. They also suggested that the KAT1 VSD is intrinsically biased by the hydrophobic pocket bordered by Phe^{102}. In effect, extending the hydrophillic cavity into the space around this residue position normally favours the 'up' state corresponding to the closed KAT1 channel.

Substitutions of the conserved acidic residue external to Phe^{102} favor the open KAT1 channel

KAT1 and its homologues retain three Asp residues within the S2 and S3 α-helices at positions that are conserved among many Kv and other voltage-gated channels [Fig. 1, see also Pless, et al. (2011)]. Of these, Asp^{95} of KAT1 aligns with the Glu^{283} of the *Shaker* K^+ channel to the outside of the central Phe residue. This acidic residue is thought to form part of the network of salt bridges with positively charged residues of the S4 α-helix (Papazian et al. 1995; Silverman et al. 2003; Long et al. 2005; Pless et al. 2011). Even the relatively conservative mutation to Gln in the *Shaker* K^+ channel results in roughly a +70 mV displacement of the conductance-voltage curve and a suppression of the current. This effect in destabilizing the 'up' relative to the 'down' state of the VSD underlines the importance of the salt bridges in an otherwise hydrophobic environment (Pless et al. 2011). Glu^{283} is positioned in close proximity to Arg^{368} and Arg^{371} of the S4 α-helix in the 'up' state of the *Shaker* channel, and these residues map to Arg^{171} and Arg^{174} in KAT1.

We used our equilibrated models in the two states of the VSD (Fig. 3A) to determine the atomic distances between these residues and the effects of Asp^{95} mutations (Table 2). Comparing values with that of KAT1^{wt} showed, for Asp^{95} mutations, that the KAT1^{D95E} and KAT1^{D95N} substitutions affect the C-C distances in the 'up' state. The most prominent effect of the KAT1^{D95E} substitution was an increase in the distances to Arg^{171} and Arg^{174} by 1.59 (36%) and 0.44 (10%) Å, respectively; for KAT1^{D95N}, the principle effects along with loss in salt-bridge formation were increases in the distances to Arg^{171} and Arg^{174}, in this case by 1.63 Å (37%) and 0.64 Å (14%), respectively, as well decreases in the solvation energies of these residues (Table 2). Thus, both mutations were predicted to favor the open KAT1 channel by reducing the efficacy of the electrostatic network in the 'up' state of the VSD.

To test these predictions, we incorporated these Asp^{95} substitutions in KAT1, expecting that these modest substitutions should favor the 'down' state of the VSD – and hence the open KAT1 channel – over a wide voltage range. As expected, when expressed in *Xenopus* oocytes KAT1^{D95E}, and to a greater extent the KAT1^{D95N} mutant, showed substantial positive-going shifts in current- and conductance-voltage characteristics compared to KAT1^{wt} (Fig. 4B). Mean KAT1^{D95E} and KAT1^{D95N} currents were well-fitted jointly with KAT1^{wt}, yielding shifts near +40 mV and +65 mV in the mid-point voltages,

respectively (Table 1). Analysis of the KAT1^{D95E} and KAT1^{D95N} current kinetics (Fig. 4C) also showed very significant decreases in relaxation halftimes at any one voltage on activation, thus parallelling the displacements of the conductance-voltage curves, and a complementary increase in the apparent time constant for current deactivation at -50 mV. These results largely parallel those of Gln^{283} substitution in the Kv1.2 channel, but without substantial change in the mean conductance maximum or gating charge δ (Pless et al. 2011). Note, too, that these substitutions had little effect on hydration predicted around Phe^{102} (Fig. 3). including to its bounding hydrophobic pocket predicted to the outside of this residue.

Substitutions of conserved acidic residues at the base of the S2 and S3 α-helices favor the open KAT1 channel

In mammalian and *Shaker* Kv channels, highly-conserved Glu and Asp residues near the cytosolic ends of the S2 and S3 α-helices are thought to form complementary electrostatic interactions with residues at the base of the S4 α-helix. In the *Shaker* channel this network most likely includes in the S4 α-helix the inner-most Lys (K5), which is represented by Arg^{177} in KAT1, and the next Arg residues (R3, R4) towards the outside, which correspond to Arg^{171} and Arg^{174} in KAT1. Acidic Glu and Asp residues that situate to the inside of the central Phe of the Kv and *Shaker* models have been suggested to form an 'occluded' site for charge coordination within the VSD (Tao et al. 2010). Substitution of the Glu and Asp residues with Gln and Asn, respectively, have a substantial effect on the conductance-voltage relations and less so on the apparent gating charge for activation in the *Shaker* channel (Papazian et al. 1995; Seoh et al. 1996). By contrast, conservative substitutions of the S3 Asp residue with Glu and with a neutral keto analogue of Asp, 2-amino-4-ketopentanoic acid, have little effect on its conductance-voltage curve (Pless et al. 2011). These latter observations have been interpreted to reflect the importance of a local, high-dielectric environment per se, rather than of charge-charge interactions with the S4 α-helix.

Residues that might be associated with a corresponding electrostatic network in KAT1^{wt} are all represented by Asp. We carried out conservative substitutions of each with Glu and expressed the mutated channels in *Xenopus* oocytes. Figure 5 summarizes the results in comparison with data for wild-type KAT1, and the analysis of C-C distances is summarized in Table 2. Comparing KAT1^{wt} to the KAT1^{D105E} and KAT1^{D105N} mutants in the

equilibrated models indicated substantial closure in the distances to Arg^{171}, by roughly 2.93 Å (27%) and 4.79 Å (44%), respectively, in the down state. The energy of electrostatic interaction with Arg^{171} decreased substantially in $KAT1^{D105E}$ and the solvation energy also decreased in the $KAT1^{D105N}$ mutant (Table 2). Both $KAT1^{D105E}$ and $KAT1^{D105N}$ mutants showed highly-significant effects on channel gating, albeit with somewhat reduced current amplitudes (Fig. 5A,B; Table 1). The conductance-voltage relations were right-shifted along the voltage axis, the $V_{1/2}$ for $KAT1^{D105E}$ and for $KAT1^{D105N}$ each displaced roughly +40 mV relative to $KAT1^{wt}$, and were parallelled by the activation and deactivation kinetics. No significant effect could be identified in gating charge for the mutants. By contrast, we observed little difference with the $KAT1^{D141E}$ mutant (Fig. 5A,B), despite the proximity of this residue to Arg^{171} in the 'down' state and its probable salt-bridge formation with Arg^{177} in the 'up' state (Fig. 5C). The $KAT1^{D141N}$ mutant failed to give a current.

Analysis of the equilibrated $KAT1^{D141E}$ substitution predicted similar effects on the C-C distances between these residues in the 'up' and 'down' states, suggesting that any impact in destabilizing the 'down' state might be compensated by a similar effect in destablizing the 'up' state, albeit through interactions with different S4 residues. To select between these interactions we targeted Arg^{177}, which is predicted to interact with Asp^{141} only in the 'up' state, reasoning that conservative substitution with a $KAT1^{R177K}$ mutant might spatially constrain salt-bridge formation in the 'up' state without affecting the electrostatic interactions of the residue in its aqueous environment in the 'down' state. Comparisons of the KAT1 models (Table 2) supported this idea, indicating the effect of the $KAT1^{R177K}$ mutant in its spacing to Asp^{141} in the 'up' state would be sufficient to reduce the energy of electrostatic interaction between these residues. Thus, we expected the $KAT1^{R177K}$ mutation to favor the 'down' state and open channel. Figure 5 and Table 1 show that, like the $KAT1^{D105E}$ mutant, $KAT1^{R177K}$ yielded a positive-going shift in the conductance-voltage curve relative to $KAT1^{wt}$ and complementary changes in the activation and deactivation kinetics. Again, the $KAT1^{R177K}$ mutant gave reduced currents, which may reflect a reduced stability of the expressed protein or its delivery to the plasma membrane. Nonetheless, the complementary effects of these two conservative substitutions is consistent in each case with a bias to the 'down' state of the KAT1 VSD that favors the open channel.

A three-state, reaction-kinetic model of KAT1 gating

The substantial effects on KAT1 gating outlined above raise the question whether the characteristics of the several mutations might be accommodated within a single, kinetic framework for channel gating. We undertook to model KAT1 gating assuming that the opening and closing of the channel are time-homogeneous stochastic processes and can therefore be described as some combination of exponential functions. Three features of the KAT1 current guided a selection of a minimum reaction-kinetic framework for a kinetic model of gating. First, KAT1 activation is weakly sigmoidal on activation but deactivation was roughly exponential, indicating the presence of at least two exponential components to current relaxations entering the open state and a single exponential component that dominated the transition to the closed state [see also Zei and Aldrich (1998) and Hoshi (1995)]. Second, all of the mutations affected the mid-point voltage $V_{1/2}$; although not a specific guide in model selection, we noted above that the mutations were without substantive effect on the apparent gating charge. Finally, each of the mutations could be connected to changes in activation and, to a greater or lesser extent, to deactivation as a function of membrane voltage. Of these features, the first is consistent with *n*-state models comprising a series of closed states that lead to one or more open states of the channel; the second and third features justify associating the primary effects of each mutation with changes in one or more of the reaction constants rather than with gating charge per se. The simplest model that satisfies all of these requirements comprises three states and four reaction constants with each of the reaction constants includes a voltage-dependent coefficient

$$C3 \underset{k_{23}}{\overset{k_{32}}{\rightleftarrows}} C2 \underset{k_{12}}{\overset{k_{21}}{\rightleftarrows}} O1 \quad . \qquad [2]$$

Here *C3* and *C2* denote two closed states that communicate serially with the open state *O1*, and the reaction constants k_{32}, k_{21}, k_{23}, and k_{12} define the transitions between states and direction as indicated by the subscript *ij*. In effect, this scheme represents a condensed form of the model resolved by Zei and Aldrich (1998) for the wild-type KAT1 channel in which

distal closed states, and the isolated 'burst' closed state are subsumed within one or the other of the two dominant states *C3* and *C2* (Gradmann et al. 1987). We introduced voltage-sensitivity to these transitions by assigning a voltage-sensitivity coefficient δ_{ij} for each reaction constant k_{ij} so that

$$k_{ij} = k_{ij}^{o} e^{\delta_{ij} u} \quad [3]$$

where the reduced voltage $u = FV/RT$, V is the voltage and F, R and T have their usual meanings. The paired exponential terms thus correspond to a series of asymmetric Eyring barriers ($\delta_{ij} \neq \delta_{ji}$).

Now at any given time t, the macroscopic current $I(t)$ comprises the sum of a steady-state component I_s and two exponential components (Bertl et al. 1988; Blatt and Gradmann 1997)

$$I(t) = I_s + I_1 e^{-\lambda_1 t} + I_2 e^{-\lambda_2 t} \quad . \quad [4]$$

The steady-state current at each voltage is given by the product of the ensemble open channel conductance g_o, the electrical driving force V-E_K from the K^+ equilibium voltage E_K, and the proportion of channels in the open state (= steady-state open probability) p_{1s}

$$I_s = g_o (V - E_K) p_{1s} \quad [5]$$

where

$$p_{1s} = \frac{k_{32} k_{21}}{b} \quad \text{and} \quad b = k_{32} k_{21} + k_{32} k_{12} + k_{12} k_{23} \quad . \quad [6a,b]$$

The two relaxation constants, λ_1 and λ_2, of Eqn. 4 denote the eigenvalues of the differential rate equations (Bertl et al. 1988; Blatt and Gradmann 1997), each equivalent to the inverse of the corresponding time constant, and are given by

$$\lambda_{1,2} = \frac{a}{2} \pm \frac{(a^2 - 4b)^{1/2}}{2} \qquad [7]$$

where $a = k_{32} + k_{23} + k_{12} + k_{21}$ and b is defined by Eqn. 5b. Finally, the current relaxation amplitudes I_1 and I_2 are defined by the changes in the relative occupation of *C2* and *O1*, that is the changes in their relative probabilities Δp_2 and Δp_1 respectively, on a step change in voltage so that

$$I_1 = \frac{\Delta p_1(k_{12} - \lambda_2) - \Delta p_2 k_{21}}{\lambda_1 - \lambda_2} g_o(V - E_K) \qquad [8a]$$

and

$$I_2 = \frac{\Delta p_1(k_{12} - \lambda_1) - \Delta p_2 k_{21}}{\lambda_2 - \lambda_1} g_o(V - E_K) \quad . \qquad [8b]$$

The ensemble, steady-state conductance-voltage characteristics for KAT1^{wt} and all of the KAT1 mutants is summarised in Fig. 6. We fitted these data to Eqn. 6. Sets of current relaxations for activation and deactivation for each of the mutants, including the data sets shown in Figs. 2, 4 and 5, were fitted to Eqn. 4 after thinning these data sets to a manageable size (see Fig. 6B and **Material and Methods**). We permitted g_o to vary for KAT1^{D105E}, KAT1^{D105N} and KAT1^{DR177K} only, because clear reductions in maximum conductance were evident for these constructs (Fig. 5); otherwise fittings to both equations were carried out jointly, with the maximum number of voltage-sensitivity coefficients and reaction constants held in common between data sets for each KAT1 construct. Thus, the strategy was to seek the minimum set of reaction constants and voltage-sensitivity coefficients that were set free between KAT1 constructs in order to satisfactorily fit all of the experimental data.

We surmised that the reaction constant k_{21} was likely to dominate transition to the open state, given the weak sigmoidicity to activation. Thus, it was not surprising that best

fittings to all of the data sets were obtained with values for k_{21} and k_{12} that dominated much of the transitions between the three states of the channel. The results are summarised, and fittings to the steady-state conductance-voltage relations and to a selection of current relaxations are shown in Figs. 6 and 7. Several general observations can be drawn from the analysis. (1) All of the data sets were well-fitted with a single set of parameter values for the voltage-sensitivity coefficients δ_{ij} (i,j = 1,2,3) common to KAT1^{wt} and all of the KAT1 mutants. The finding is consistent with the earlier Boltzmann analyses indicating that the various mutations affected primarily the mid-point voltage $V_{1/2}$ and had little or no influence on the apparent gating charge. The total charge associated with gating [= $\Sigma(\delta_{ij})$, for i,j=1,2,3] was 3.29e^-, which is roughly twice the apparent gating charge indicated from the Boltzmann analysis (Table 1) and highlights the difficulties in relating the Boltzmann parameters to a mechanism when channel gating is not a simple two-state process. The value is close to the 3.42e^- estimated by Zei and Aldrich (1998), who also noted the much lower values derived from Boltzmann analysis. (2) All fittings indicated the predominant distribution of voltage-sensitivities between reaction constants k_{32}, k_{21} and k_{12}, with values for δ_{23} comprising less than 0.01 percent of the total charge associated with gating. Virtually identical results were obtained when k_{23} was voltage independent (δ_{23}=0). These findings indicate a voltage dependence in deactivation determined entirely by the initial transition out of the open state *O1* and the balance of the reaction constants k_{12} and k_{21}; by contrast, the voltage dependence in activation was spread between both transitions leading into the open state of the channel. (3) Current kinetics and conductances were well-fitted with only k_{21}^o varying between KAT1^{wt}, KAT1^{D95E}, KAT1^{D95N}, KAT1^{D105E}, KAT1^{D105N}, KAT1^{R177K} and KAT1^{D141E} (Figs. 6 and 7). In kinetic terms, the primary effect of these mutations was on the rates of transition into the open state of the channel. (4) Finally, currents and conductances for KAT1^{F102W}, KAT1^{F102Q}, KAT1^{F102S} and KAT1^{F102L} with KAT1^{wt} were well-fitted only with both k_{21}^o and k_{12}^o varying between data sets, in other words with the intrinsic rates both for entry to and exit from the open state determining the differences between the KAT1 constructs. These last two observations highlight the substantially different consequences of the two groups of mutations on KAT1 gating and we return to this point below.

DISCUSSION

The KAT1 K^+ channel is one of a family of nine transmembrane K^+ channel proteins in Arabidopsis, the members of which share many of the hallmarks of the Kv superfamily of K^+ channels found in mammals and in *Drosophila* (Very and Sentenac 2003; Dreyer and Blatt 2009). Although little is known of the molecular mechanics of gating in the plant Kv-like channels, there are many similarities implicated in coupling the charge-driven movements of the voltage-sensor domains (VSDs), to the opening of the channel pore. The VSD conformation of KAT1, when closed, appears to correspond closely with VSD conformations, often referred to the 'up' state, associated with the open *Shaker* and mammalian Kv K^+ channels (Latorre et al. 2003; Lai et al. 2005). Whereas the latter rectify outward, opening at positive-going voltages, KAT1 rectifies inward and gates open at voltages negative-going from approximately -100 to -120 mV. Thus, similar VSD conformations are likely for KAT1 as for the *Shaker* and Kv channels, albeit associated with the opposing states of the KAT1 channel (Dreyer and Blatt 2009). Significantly, the VSDs of the *Shaker* and mammalian Kv channels incorporate five, positively charged residues spaced at regular intervals along the fourth transmembrane α-helix. Movement of these residues within the transmembrane electric field lead to the conformational changes that drive channel gating with voltage (Dreyer and Blatt 2009; Palovcak et al. 2014). Although only four of these residues are conserved in KAT1, their charges must nonetheless be coordinated by a network of counter-charges within the VSD structure. It has been thought likely, therefore, that the VSD of KAT1 should incorporate an electrostatic network similar to the *Shaker* and mammalian models (Palovcak et al. 2014). This supposition had gone untested by mutational analysis to probe the conformational dynamics of the KAT1 VSD itself, but is clearly central to understanding channel function as a target for future manipulation.

Here we report a set of conserved residues within the KAT1 VSD that are likely to contribute to a network of electrostatic charge-charge interactions during gating. Our data indicate substantial parallels with electrostatic networks of the *Shaker* and mammalian Kv channel VSDs. In particular, they are consistent with two electrostatic interaction centers either side of a conserved Phe residue within the S2 α-helix and positioned roughly mid-way across the membrane. The data nonetheless demonstrate a negative shift in the KAT1 gating characteristic as the default when this central aromatic residue is removed. The observations

suggest a bias in KAT1 that favors the 'up' state of the VSD and closed channel when this region within the VSD is hydrated, and they point to an occluded, hydrophobic pocket located to the outside of the conserved Phe residue. This interpretation is consistent also with an analysis of KAT1 gating that highlights the distinct kinetic effects of mutations within the putative electrostatic coordination centers compared to those of the central Phe residue. Finally, the observations demonstrate the feasibility of manipulating the gating of a plant Kv-like K^+ channel over the physiological voltage range commonly found at the plant plasma membrane.

Acidic residues of the KAT1 S2 and S3 α-helices identify two charge-coordination centers

In the absence of a crystal structure for any plant K^+ channel, previously we mapped the Arabidopsis Kv-like channels to the mammalian Kv1.2 (Gajdanowicz et al. 2009; Riedelsberger et al. 2010; Garcia-Mata et al. 2010; Gonzalez et al. 2012) and the KvaP K^+ channel structures (Johansson et al. 2006). These studies proved successfully in predicting structural features of the plant channels, including access of water-soluble reagents within the VSD of the outward-rectifying channel SKOR (Garcia-Mata et al. 2010). Our extension of the KAT1 model in the present work underscores the fundamental structural similarities between KAT1 and the Kv and *Shaker* K^+ channels. Again, as template we used the same *ab initio* model built from the α-subunit of Kv1.2, including the VSD as well as the α-helices forming the pore, that yielded conformations compatible with experimental analysis of KAT1 (Grabe et al. 2007; Gajdanowicz et al. 2009; Riedelsberger et al. 2010). Most important, these simulations point to key roles for acidic residues within the S2 and S3 α-helices that are important for stabilizing the VSD between the 'up' and 'down' states previously associated with KAT1 gating (Latorre et al. 2003; Lai et al. 2005). Of these, Asp^{105} and Asp^{141} map to the inside of Phe^{102}, and are predicted to interact, alternately between the 'up' and 'down' states, with Arg^{177} and Arg^{174} on the S4 α-helix (Fig. 5); Asp^{95} maps to the outside of Phe^{102} and interacts with Arg^{174} and Arg^{171} in the 'up' state, and with Arg^{165} in the 'down' state (cf. Figs. 4 and 5). Indeed, the KAT1 model offered consistent and appropriate explanations for each of the mutations we introduced and analyzed experimentally at these sites (Figs. 3-5, Supplemental Figs. S1-S3, Tables 1 and 2). Thus, like the mammalian Kv and *Shaker* channels (Papazian et al. 1995; Tao et al. 2010; Pless et al. 2011; Schwaiger et

al. 2013), the VSD of KAT1 appears to describe a pair of counter charge-interaction centers that are positioned, one on either side of the 'pivot' formed by Phe^{102}.

Our studies also reinforce the counterpoint with the mammalian Kv and *Shaker* K^+ channels, implicit in earlier studies of KAT1. The Kv1.2 and *Shaker* channels open with positive-going voltages that drive the VSD into the 'up' state. This state exposes residues of the S4 α-helix otherwise buried within the membrane to modification by aqueous cysteine-reactive, methanethiosulfonate reagents from the outside and hides others on the inside on channel opening (Larsson et al. 1996), and it aligns key residues in the S4 α-helix in close proximity with amino acids near the outer surface of the S5 α-helix (Elinder et al. 2001). The same conformation in the KAT1 VSD has been associated with the closed channel (Latorre et al. 2003; Lai et al. 2005): for example, residues in the S4 α-helix move inward toward the cytosol (the 'down' position), becoming inaccessible to the same membrane-impermeant reagents outside when the channels *open* at negative-going voltages (Latorre et al. 2003) and amino acids that pack against the S5 α-helix at negative voltages in the open conformation of KAT1 correspond with residues in the *Shaker* and Kv1.2 K^+ channels which are similarly positioned, but in the closed channel conformation (Lai et al. 2005). A similar picture now emerges for the electrostatic charge-interaction centers. Like recent studies of the *Shaker* channel and Kv1.2/2.1 chimera (Pless et al. 2011; Schwaiger et al. 2013), we found that manipulations disturbing the charge-charge interactions at these centers favored the 'down' state of the VSD and a positive-going displacement of the midpoint voltage for channel gating (Figs. 4 and 5, Table 1). Significantly, these substitutions had little effect on the hydration surface within the VSD, indeed modestly increasing its hydrophobicity in the $KAT1^{R177K}$ mutant (Fig. 3). It follows that the KAT1 VSD is biased to the 'down' conformation by these manipulations independent of any substantive action on hydration around the Phe^{102} and the hydrophobic pocket it bounds within the VSD. Furthermore, for KAT1 the result is to extend the voltage range for channel activity across almost the entire physiological voltage range typical of the plant cell.

Whether the same characteristics apply to the other Arabidopsis Kv-like channels, including KAT2, KC1 (KAT3), AKT1 and the outward-rectifying K^+ channels GORK and SKOR (Dreyer and Blatt 2009), remains to be seen. Nonetheless, alignments and the topology of these channels indicates a remarkably high degree of sequence conservation,

including the absolute conservation of residues contributing to the charge interaction centers and their separation by a central Phe (cf. Fig. 1). Furthermore, a related molecular-dynamic model of the SKOR K^+ channel has yielded a very similar pattern of hydration around the S4 α-helix, correctly predicting residue availability for MTS and redox modifications and their voltage-dependence (Garcia-Mata et al. 2010). Thus, it is most likely that analysis of the charge interaction centers in the VSDs of these channels will yield results very similar, if not identical, to those we describe here.

Biasing the KAT1 VSD for channel closure

We began these studies in part to identify VSD mutations that affect the effective voltage range for gating and might thus be used in manipulating K^+ transport. Following Tao, et al. (2010), our initial efforts focused on Phe^{102} of KAT1. Like the earlier study, we found that gating of the $KAT1^{F102W}$ mutant was displaced strongly negative-going from $KAT1^{wt}$ (Fig. 2 and 6), consistent with a change in total gating energy in excess of 8 kJ. Unlike Tao, et al. (2010), every other mutation we introduced at this site led to negative-going shifts in the current- and conductance-voltage relations of the channel. Even the $KAT1^{F102Q}$ and $KAT1^{F102S}$ substitutions yielded strong, negative-going displacements in channel gating. Indeed, the characteristics of the KAT1 VSD are at odds with the the mammalian Kv and *Shaker* models in this respect. Tao, et al. (2010) observed that substituting the final, positively-charged residue, a Lys (K5), on the S4 α-helix with Arg led to a reversal in the effects of Phe substitution with Trp: whereas $V_{1/2}$ shifted negative with Trp in the K5 form of the channel, it was displaced to more positive voltages in the R5 form of the channel. By contrast, in KAT1 this final residue of the S4 α-helix occurs naturally as Arg, yet the effect of the $KAT1^{F102W}$ mutation are very similar – and qualitatively identical – to the Phe-to-Trp substitution in the K5 model of the mammalian VSD. A similar disjuncture is evident in the effects of the $KAT1^{R177K}$ mutant itself: this substitution led to a substantial negative shift in $V_{1/2}$ for the Kv1.2/2.1 chimera, but in KAT1 the effect was to displace $V_{1/2}$ by roughly +60 mV (Figs. 5 and 6).

How might we understand both the similarities and differences from the mammalian Kv and *Shaker* channels? Molecular dynamic simulations of the KAT1 models point to an occluded, hydrophobic pocket to the outside of Phe^{102}, with hydration of the S4 α-helix to the

inside of Phe^{102} which is enhanced in the 'down' (open channel) state. Comparison of the several mutants predicted a further hydration around and beyond position 102 with each of the Phe^{102} substitutions, but with little or no effect following mutations associated with the charge interaction centers (Fig. 3, Supplemental Fig. S3). A straightforward interpretation, again, is that dehydration of the S4 surface around this outer, occluded pocket is an important factor in VSD conformation associated with the 'up' state and its hydration favors the 'down' state. It follows, too, that the effects of the charge-interaction centers are mechanistically distinct, as noted above. In effect, in KAT1 Phe^{102} may be seen to maintain a low dielectric barrier that helps immobilize Arg^{171} in the 'down' state and facilitates transfer of Arg^{177} beyond this hydrophobic barrier. This interpretation concurs with the recent studies of the Shaker channel and Kv1.2/2.1 chimera (Pless et al. 2011; Schwaiger et al. 2013), noted above. It echos the suggestion of Lacroix and Bezanilla (2011) that the conserved Phe in the *Shaker* K^+ channel forms a hydrophobic barrier, and findings of a substantial increase in aqueous accessibility to the inner half of the S4 α-helix on HCN1 channel opening (Bell et al. 2004). It also suggests that the detail of the VSD transition for KAT1 differs from that of the Kv and *Shaker* models in its strong dependence on a hydration/dehydration transition rather than on interactions of the K5 Lys residue with π-electron cloud formed by the aromatic ring at position 102 (Pless et al. 2011; Schwaiger et al. 2013). In short, the KAT1 VSD appears inherently biased to the 'up' state; this bias is normally countered by hydration of the S4 residues to the inside of Phe^{102}. Manipulations that extend S4 hydration into the outer pocket beyond Phe^{102} stabilize the 'up' state and, hence, the closed KAT1 channel.

A model for KAT1 gating

This molecular dynamic interpretation also finds parallels with a reaction-kinetic analysis of KAT1 gating (Figs. 6 and 7). The analysis showed that a satisfactory approximation to the experimental data was realized with a serial, three-state model of gating. A systematic comparison with the six-state model arrived at by Zei and Aldrich (1998) is not possible, in the first instance because the latter incorporated an isolated closed state to account for voltage-dependent periods of high activity, so-called 'bursting' behavior, that was identified in single-channel recordings. This behavior, as well as the longer-lived closed lifetimes, cannot be isolated in whole-cell measurements such as we have undertaken.

So, expanding our model beyond the three states of Scheme 1 (above) is not justified and would result in a system of gating states with substantial indetermination. Even so, this three-state analysis highlights a substantial difference in the kinetic effects of the two sets of mutations. Specifically, mutations targeted to Phe^{102} were successfully accommodated by coordinate and antiparallel changes to the values for k_{21}^{o} and k_{12}^{o}; assigning the effects of substitutions at this site to a single reaction constant, or to any other combinations of paired reaction constants, was unsatisfactory. By contrast, mutations at sites associated with the electrostatic charge centers to the inside and outside of Phe^{102} were well-fitted with k_{21}^{o} only varying between data sets for the various mutants. Again, assigning the effects of these substitutions to any other single reaction constant was uniformly unsatisfactory.

Connecting these specific kinetic constants with the dynamics of the VSD conformational transitions is not possible with the information available at present. Nonetheless, the comparison allows one set of parallels to be drawn: mutations of Phe^{102} predicted to effect changes in water access to the hydrophobic pocket in the VSD also associate with kinetic effects on transitions both in and out of the open state of the channel, and they favor the 'up' state of the VSD; mutations of the electrostatic coordination centers predicted to have little or no effect on hydration within the VSD associate principally with the kinetics of transition into the open state of the channel, and they favor the 'down' state of the VSD. In general, these findings now add to a picture of the mechanics in K^+ channel gating, providing evidence for network of centers coordinating charge between the α-helices in the 'up' and 'down' states of the KAT1 VSD analogous to those in other Kv channels (Dreyer and Blatt 2009). In short, voltage drives the gating process in this inward-rectifying K^+ channel much as it does in the outward-rectifying channels characterized by the Kv and *Shaker* models, at least to the extent of the 'handover' of positively-charged Arg residues between two, putative electrostatic charge interaction centers associated with a set of highly-conserved, acidic residues that localize to the S2 and S3 α-helices and either side of Phe^{102} of KAT1.

Finally, our studies highlight KAT1 as a model in a very practical sense. Previous development of a quantitative systems platform for the premier plant cell model of the guard cell had shown substantial predictive power in guiding experiments (Wang et al. 2012; Hills et al. 2012; Chen et al. 2012b). A recent analysis using this platform indicated that simple

manipulations of the population of ion channels at the plasma membrane and tonoplast are unlikely to have a substantial effect on cellular homeostasis and guard cell function, unlike manipulations of the primary, energy-coupled transporters including the plasma membrane H^+-ATPase (Lawson and Blatt 2014; Wang et al. 2014a). This prediction has found independent verification in a concurrent study (Wang et al. 2014b) reporting that overexpressing several K^+ channels in guard cells of Arabidopsis had no measurable effect on stomatal behavior. The latter study reported a small increase in stomatal aperture and assimilation with a 3-fold increase in expression of AHA2, one of the three dominant H^+-ATPases at the guard cell plasma membrane, albeit with a substantial cost in water use by the plant. By contrast, from their systems analysis Wang, et al. (2014a) concluded that even small changes of ±18 mV to the $V_{1/2}$ for gating of one or both the inward- and outward-rectifying K^+ channels, including KAT1, could influence stomatal kinetics without a cost in water use efficiency. The present results establish the feasibility of such manipulations, demonstrating that single point mutations within the KAT1 VSD are sufficient to drive $V_{1/2}$ across most, if not all of the physiological voltage range, from values in excess of -200 mV to near -50 mV. We anticipate that these findings will underpin future efforts towards engineering plant membrane transport for improved efficiencies in mineral and water use in the field.

MATERIAL AND METHODS

Molecular biology

Open-reading frames for *KAT1* were amplified with gene-specific primers including Gateway attachment sites (*att*B1/*att*B2). A subsequent BP-reaction in pDONR207 (Invitrogen, Carlsbad USA) yielded entry clones that were verified via sequencing. Point mutants were generated by site-directed mutagenesis with SDM-Assist (Karnik et al. 2013). Gateway Destination clones were generated using LR clonase II (Invitrogen) by LR reaction as described previously (Grefen et al. 2010b) in the oocyte expression vector pGT-Dest(Honsbein et al. 2009; Chen et al. 2011).

Electrophysiology

Electrical recordings were carried out with KAT1 constructs as described previously (Honsbein et al. 2009; Grefen et al. 2010a). Coding sequences for wild-type and point mutants were cloned in pGT-Dest (Grefen et al. 2010a) and capped cRNA synthesised in vitro using T7 mMessage mMachine (Ambion, Austin TX). cRNA quality as a single band was confirmed by denaturing gel electrophoresis. To ensure uniform injections of KAT1 transcript, mixtures were made up to a standard volume as necessary with RNAse-free water.

Stage VI oocytes were isolated from mature *Xenopus laevis* and the follicular cell layer was digested with 2 mg/ml collagenase (type 1A, Sigma) for 1 h. Injected oocytes were incubated in ND96 (96 mM NaCl, 2 mM KCl, 1 mM $MgCl_2$, 1 mM $CaCl_2$, 10 mM HEPES-NaOH, pH 7.4) supplemented with gentamycin (5 μg/ml) at 18^{o}C for three days. Whole cell currents were recorded under voltage clamp using an Axoclamp 2B (Axon Instruments, CA, USA) two-electrode clamp circuit (Vergani et al. 1998; Leyman et al. 1999; Sutter et al. 2006). Measurements were carried out under continuous perfusion either with 30 mM KCl and 66 mM NaCl or with 96 mM KCl with the addition of 1.8 mM $MgCl_2$, 1.8 mM $CaCl_2$ and 10 mM HEPES-NaOH, pH 7.2. Recordings were analyzed and leak currents subtracted using standard methods (Leyman et al. 1999; Sutter et al. 2006) with Henry IV software (Hills and Volkov 2004) (Y-Science, University of Glasgow, Glasgow UK).

Molecular dynamic simulations

Molecular dynamic (MD) simulations were carried out with the wild-type sequence and with the corresponding residue substitutions, first using the NAMD program (Phillips et al. 2005) and the CHARMM27 forcefield (MacKerell et al. 1998). Open and closed models were embedded within a lipid bilayer in a periodic boundary condition box with water molecules, K^+ and Cl^- ions, optimized using energy minimization followed by equilibration at 298 K for 5 ns with a harmonic restraint of 0.5 kcal/mol $Å^2$ applied to the backbone atoms (Gajdanowicz et al. 2009). Distances were analysed between terminal residue carbons and salt bridge formation assessed using the VMD 'salt bridge' plug-in (www.ks.uiuc.edu/Research/vmd/plugins/saltbr/).

We used the entire α-subunit of Kv1.2 obtained by the Rosseta method as the template for KAT1 (Gajdanowicz et al. 2009), and selected the single subunit in each MD simulation of KAT1 and the mutants that yielded most of the interactions reported for the Kv1.2 channel. The model of KAT1, with the VSD in the 'up' and 'down' states, was derived *ab initio* with Rossetta (Yarov-Yarovoy et al. 2006) and is compatible with experimental analysis of the KAT1 'down' state (Grabe et al. 2007) using the sequence alignment of Pathak, et al. (2007). We omitted from homology mapping residues Y^{114}-K^{126} of the extended S2-S3 cytoplasmic loop of KAT1 that is not present in the Kv1.2 sequence. Residues P^{148}-S^{160} between the S3 and S4 α-helices were assigned to the external loop which, in Kv1.2, includes an additional eleven amino acids. Further information is provided in Supplemental Fig. 1. Following the naming convention for the key charged residues of the VSD (Vargas et al. 2011) in KAT1, the basic residues of the S4 α-helix, R1, R3, R4, and K5, correspond to Arg^{165}, Arg^{171}, Arg^{174}, and Arg^{177}. Residue R2 is not present in KAT1 channel. The acidic residues E1 and E2 of the S2 α-helix correspond to Asp^{95} and Asp^{105}, respectively, and D3 of the S3 α-helix, corresponds to Asp^{141}. In the 'up' state conformation, the interactions are formed between R3 and E1 (Pless et al. 2011), R4 and E1, and between K5 and D3 (Tiwari-Woodruff et al. 2000). In the 'down' state conformation, R1 interacts with E1, and R3 interacts with E2 and D3 (Khalili-Araghi et al. 2010). Each subunit was assembled within a homotetramer and embedded in a periodic boundary condition box (above), and was optimized using energy minimization followed by equilibration at 300^o K for 10 ns. Harmonic restraints of 50 kcal/mol $Å^2$ were applied to R1, R3, R4, K5, E1, E2 and D3 to reproduce experimental interactions. The rest of the protein structure was without

harmonic restraints during MD simulations. This second part of MD simulations was carried out using Desmond software (Desmond Molecular Dynamics System, Version 2.2) (Bowers et al. 2006) and OPLS2005 forcefield (Kaminski et al. 2001).

Reaction-kinetic modelling

For quantitative analysis of KAT1 gating, mean steady-state conductance-voltage relationships and sets of current traces for each of the various KAT1 constructs were fitted jointly using a Marquardt-Levenberg algorithm and least-squares minimization (Marquardt 1963; Press et al. 1986) to the serial (pseudo-) three-state system described by Scheme 1. The differential equations for this model have been described previously (Bertl et al. 1988; Blatt and Gradmann 1997) and their solution yields Eqns. 3-8. Steady-state conductances were fitted to Eqn. 4 and current relaxations were fitted to Eqn. 6, allowing a minimum of parameter values to vary between data sets representing each of the KAT1 constructs. Data sets representing current relaxations were thinned to a manageable size by selecting values at regular time intervals to give a total of approximately 1000 data points per set, and residuals were adjusted to give equal weighing between data points within traces and between curves within each data set. Numerical values for each of the joint parameters were sought by sequential adjustment from starting values and analyses were repeated after initializing with different starting values to ensure that fittings convered on a single solution.

Statistics

Statistical analysis of independent experiments is reported as means ±SE as appropriate with significance determined by Student's t-test or ANOVA. Joint non-linear least-squares fittings were carried out using a Marquardt-Levenberg algorithm (Marquardt 1963) implemented in SigmaPlot v.11 (SPSS, Chicago USA).

Acknowledgements We are grateful to George Boswell for help with *Xenopus* maintenance and to Osvaldo Yáñez for help with MD analysis. This work was supported by grants BB/H001673/1, BB/H024867/1, BB/H009817/1 and BB/K015893/1 from the UK Biotechnology and Biological Sciences Research Council to MRB, ANILLO grant ACT1104

to WG and JR, and by grant DR430/8-1 from the Deutsche Forschungsgemeinschaft to ID, WG and JR.

References:

1. Alves CN, Marti S, Castillo R, Andres J, Moliner V, Tunon I, Silla E (2007) Calculation of binding energy using BLYP/MM for the HIV-1 integrase complexed with the S-1360 and two analogues. Bioorganic & Medicinal Chemistry 15: 3818-3824

2. Amtmann A, Blatt MR (2009) Regulation of macronutrient transport. New Phytol 181: 35-52

3. Becker D, Dreyer I, Hoth S, Reid JD, Busch H, Lehnen M, Palme K, Hedrich R (1996) Changes in voltage activation, Cs^+ sensitivity, and ion permeability in H5 mutants of the plant K^+ channel KAT1. Proc Natl Acad Sci USA 93: 8123-8128

4. Bell DC, Yao H, Saenger RC, Riley JH, Siegelbaum SA (2004) Changes in local S4 environment provide a voltage-sensing mechanism for mammalian hyperpolarization-activated HCN channels. J Gen Physiol 123: 5-19

5. Bertl A, Klieber HG, Gradmann D (1988) Slow kinetics of a potassium channel in acetabularia. J Membr Biol 102: 141-152

6. Blatt MR (1988) Potassium-dependent bipolar gating of potassium channels in guard cells. J Membr Biol 102: 235-246

7. Blatt MR, Gradmann D (1997) K^+ -sensitive gating of the K^+ outward rectifier in *Vicia* guard cells. J Membr Biol 158: 241-256

8. Bowers KJ, Chow E, Xu H, Dror RO, Eastwood MP, Gregersen BA. Scalable algorithms for molecular dynamics simulations on commodity clusters. 84. 2006. Tampa, FL, ACM. Proceedings o fthe 2006 ACM/IEEE Conference on Supercomputing.
Ref Type: Conference Proceeding

9. Chen ZH, Grefen C, Donald N, Hills A, Blatt MR (2011) A bicistronic, Ubiquitin-10 promoter-based vector cassette for transient transformation and functional analysis of membrane transport demonstrates the utility of quantitative voltage clamp studies on intact *Arabidopsis* root epidermis. Plant Cell And Environment 34: 554-564

10. Chen ZH, Eisenach C, Xu XQ, Hills A, Blatt MR (2012a) Protocol: optimised electrophyiological analysis of intact guard cells from Arabidopsis. Plant Methods 8: 15-25

11. Chen ZH, Hills A, Baetz U, Amtmann A, Lew VL, Blatt MR (2012b) Systems Dynamic Modeling of the Stomatal Guard Cell Predicts Emergent Behaviors in Transport, Signaling, and Volume Control. Plant Physiol 159: 1235-1251

12. Daram P, Urbach S, Gaymard F, Sentenac H, Cherel I (1997) Tetramerization of the AKT1 plant potassium channel involves its C-terminal cytoplasmic domain. EMBO J 16: 3455-3463

13. Doyle DA, Cabral JM, Pfuetzner RA, Kuo AL, Gulbis JM, Cohen SL, Chait BT, MacKinnon R (1998) The structure of the potassium channel: Molecular basis of K^+ conduction and selectivity. Science 280: 69-77

14. Dreyer I, Blatt MR (2009) What makes a gate? The ins and outs of Kv-like K^+ channels in plants. Trends Plant Sci 14: 383-390

15. Eisenach C, Chen ZH, Grefen C, Blatt MR (2012) The trafficking protein SYP121 of Arabidopsis connects programmed stomatal closure and K^+ channel acivity with vegetative growth. Plant J 69: 241-251

16. Elinder F, Mannikko R, Larsson HP (2001) S4 charges move close to residues in the pore domain during activation in a K channel. J Gen Physiol 118: 1-10

17. Gajdanowicz P, Garcia-Mata C, Sharma T, Gonzalez W, Morales-Navarro SE, Gonzalez-Nilo FD, Gutowicz J, Mueller-Roeber B, Blatt MR, Dreyer I (2009) Distributed structures determine K^+ and voltage dependent gating of the K_{in} channel KAT1 and the K_{out} channel SKOR. New Phytol 182: 380-391

18. Garcia-Mata C, Wang JW, Gajdanowicz P, Gonzalez W, Hills A, Donald N, Riedelsberger J, Amtmann A, Dreyer I, Blatt MR (2010) A Minimal Cysteine Motif Required to Activate the SKOR K^+ Channel of *Arabidopsis* by the Reactive Oxygen Species H_2O_2. J Biol Chem 285: 29286-29294

19. Gonzalez W, Riedelsberger J, Morales-Navarro SE, Caballero J, zate-Morales JH, Gonzalez-Nilo FD, Dreyer I (2012) The pH sensor of the plant K^+-uptake channel KAT1 is built from a sensory cloud rather than from single key amino acids. Biochemical Journal 442: 57-63

20. Grabe M, Lai HC, Jain M, Jan YN, Jan LY (2007) Structure prediction for the down state of a potassium channel voltage sensor. Nature 445: 550-553

21. Gradmann D, Kleiber H-G, Hansen U-P (1987) Reaction kinetic parameters for ion transport from steady-state current-voltage curves. Biophys J 51: 569-585

22. Grefen C, Chen ZH, Honsbein A, Donald N, Hills A, Blatt MR (2010a) A Novel Motif Essential for SNARE Interaction with the K^+ Channel KC1 and Channel Gating in *Arabidopsis*. Plant Cell 22: 3076-3092

23. Grefen C, Donald N, Hashimoto K, Kudla J, Schumacher K, Blatt MR (2010b) A ubiquitin-10 promoter-based vector set for fluorescent protein tagging facilitates temporal stability and native protein distribution in transient and stable expression studies. Plant J 64: 355-365

24. Hills A, Volkov V (2004) Electrophysiology equipment and software. In MR Blatt, ed, Membrane Transport in Plants, Ed 1 Vol 15. Blackwell, Oxford, pp 40-71

25. Hills A, Chen ZH, Amtmann A, Blatt MR, Lew VL (2012) OnGuard, a Computational Platform for Quantitative Kinetic Modeling of Guard Cell Physiology. Plant Physiol 159: 1026-1042

26. Honsbein A, Sokolovski S, Grefen C, Campanoni P, Pratelli R, Paneque M, Chen ZH, Johansson I, Blatt MR (2009) A Tripartite SNARE-K^+ Channel Complex Mediates in Channel-Dependent K^+ Nutrition in *Arabidopsis*. Plant Cell 21: 2859-2877

27. Hoshi T (1995) Regulation of voltage-dependence of the KAT1 channel by intracellular factors. J Gen Physiol 105: 309-328

28. Jensen MO, Jogini V, Borhani DW, Leffler AE, Dror RO, Shaw DE (2012) Mechanism of Voltage Gating in Potassium Channels. Science 336: 229-233

29. Jiang YX, Lee A, Chen JY, Ruta V, Cadene M, Chait BT, MacKinnon R (2003) X-ray structure of a voltage-dependent K^+ channel. Nature 423: 33-41

30. Johansson I, Wulfetange K, Poree F, Michard E, Gajdanowicz P, Lacombe B, Sentenac H, Thibaud JB, Mueller-Roeber B, Blatt MR, Dreyer I (2006) External K^+ modulates the activity of the *Arabidopsis* potassium channel SKOR via an unusual mechanism. Plant J 46: 269-281

31. Kaminski GA, Friesner RA, Tirado-Rives J, Jorgensen WL (2001) Evaluation and reparametrization of the OPLS-AA force field for proteins via comparison with accurate quantum chemical calculations on peptides. Journal of Physical Chemistry B 105: 6474-6487

32. Karnik A, Karnik R, Grefen C (2013) SDM-Assist software to design site-directed mutagenesis primers introducing "silent" restriction sites. Bmc Bioinformatics 14:

33. Khalili-Araghi F, Jogini V, Yarov-Yarovoy V, Tajkhorshid E, Roux B, Schulten K (2010) Calculation of the Gating Charge for the Kv1.2 Voltage-Activated Potassium Channel. Biophysical Journal 98: 2189-2198

34. Kuo AL, Gulbis JM, Antcliff JF, Rahman T, Lowe ED, Zimmer J, Cuthbertson J, Ashcroft FM, Ezaki T, Doyle DA (2003) Crystal structure of the potassium channel KirBac1.1 in the closed state. Science 300: 1922-1926

35. Lacroix J, Halaszovich CR, Schreiber DN, Leitner MG, Bezanilla F, Oliver D, Villalba-Galea CA (2011) Controlling the Activity of a Phosphatase and Tensin Homolog (PTEN) by Membrane Potential. J Biol Chem 286: 17945-17953

36. Lacroix JJ, Bezanilla F (2011) Control of a final gating charge transition by a hydrophobic residue in the S2 segment of a K^+ channel voltage sensor. Proc Natl Acad Sci USA 108: 6444-6449

37. Lai HC, Grabe M, Jan Y-N, Jan LY (2005) The S4 voltage sensor packs against the pore domain in the KAT1 voltage-gated potassium channel. Neuron 47: 395-406

38. Larsson HP, Baker OS, Dhillon DS, Isacoff EY (1996) Transmembrane movement of the Shaker K+ channel S4. Neuron 16: 387-397

39. Latorre R, Olcese R, Basso C, Gonzalez C, Munoz F, Cosmellli D, Alvarez O (2003) Molecular coupling between voltage sensor and pore opening in the *Arabidopsis* inward rectifier K^+ channel KAT1. J Gen Physiol 122: 459-469

40. Lawson T, Blatt MR (2014) Size, speed and responsiveness of stomata impact on photosynthesis and water use efficiency. Plant Physiol 164: 1556-1570

41. Leyman B, Geelen D, Quintero FJ, Blatt MR (1999) A tobacco syntaxin with a role in hormonal control of guard cell ion channels. Science 283: 537-540

42. Lins L, Thomas A, Brasseur R (2003) Analysis of accessible surface of residues in proteins. Protein Science 12: 1406-1417

43. Long SB, Campbell EB, MacKinnon R (2005) Voltage sensor of Kv1.2: structural basis of electromechanical coupling. Science 309: 903-908

44. MacKerell AD, Bashford D, Bellott M, Dunbrack RL, Evanseck JD, Field MJ, Fischer S, Gao J, Guo H, Ha S, Joseph-McCarthy D, Kuchnir L, Kuczera K, Lau FTK, Mattos C, Michnick S, Ngo T, Nguyen DT, Prodhom B, Reiher WE, Roux B, Schlenkrich M, Smith JC, Stote R, Straub J, Watanabe M, Wiorkiewicz-Kuczera J, Yin D, Karplus M (1998) All-atom empirical potential for molecular modeling and dynamics studies of proteins. Journal of Physical Chemistry B 102: 3586-3616

45. Marquardt D (1963) An algorithm for least-squares estimation of nonlinear parameters. J Soc Ind Appl Math 11: 431-441

46. Nakamura RL, Anderson JA, Gaber RF (1997) Determination of key structural requirements of a K^+ channel pore. J Biol Chem 272: 1011-1018

47. Obermeyer G, Armstrong F, Blatt MR (1994) Selective block by α-dendrotoxin of the K^+ inward rectifier at the *Vicia* guard cell plasma membrane. J Membr Biol 137: 249-259

48. Palovcak E, Delemotte L, Klein ML, Carnevale V (2014) Evolutionary imprint of activation: The design principles of VSDs. Journal of General Physiology 143: 145-156

49. Papazian DM, Schwarz TL, Tempel BL, Jan YN, Jan LY (1987) Cloning of genomic and complementary DNA from Shaker, a putative potassium channel gene from Drosophila. Science 237: 749-753

50. Papazian DM, Shao XM, Seoh SA, Mock AF, Huang Y, Wainstock DH (1995) Electrostatic interactions of S4 voltage sensor in shaker K^+ channel. Neuron 14: 1293-1301

51. Pathak MM, Yarov-Yarovoy V, Agarwal G, Roux B, Barth P, Kohout S, Tombola F, Isacoff EY (2007) Closing in on the resting state of the shaker K+ channel. Neuron 56: 124-140

52. Phillips JC, Braun R, Wang W, Gumbart J, Tajkhorshid E, Villa E, Chipot C, Skeel RD, Kale L, Schulten K (2005) Scalable molecular dynamics with NAMD. Journal of Computational Chemistry 26: 1781-1802

53. Pilot G, Pratelli R, Gaymard F, Meyer Y, Sentenac H (2003) Five-group distribution of the shaker-like K+ channel family in higher plants. Journal of Molecular Evolution 56: 418-434

54. Pless SA, Galpin JD, Niciforovic AP, Ahern CA (2011) Contributions of counter-charge in a potassium channel voltage-sensor domain. Nature Chemical Biology 7: 617-623

55. Pongs O, Kecskemethy N, Muller R, Krahjentgens I, Baumann A, KILTZ HH, CANAL I, Llamares S, Ferrus A (1988) SHAKER encodes a family of putative potassium chanel proteins in the nervous system of *Drosophila*. EMBO J 7: 1087-1096

56. Press W, Flannerly B, Teukolsky S, Vetterling W (1986) Numerical Recipies: The Art of Scientific Computing. Cambridge University Press, Cambridge,

57. Quintero FJ, Blatt MR (1997) A new family of K^+ transporters from *Arabidopsis* that are conserved across phyla. FEBS Lett 415: 206-211

58. Riedelsberger J, Sharma T, Gonzalez W, Gajdanowicz P, Morales-Navarro SE, Garcia-Mata C, Mueller-Roeber B, Gonzalez-Nilo FD, Blatt MR, Dreyer I (2010) Distributed Structures Underlie Gating Differences between the K_{in} Channel KAT1 and the K_{out} Channel SKOR. Molecular Plant 3: 236-245

59. Rubio F, Nieves-Cordones M, Aleman F, Martinez V (2008) Relative contribution of AtHAK5 and AtAKT1 to K+ uptake in the high-affinity range of concentrations. Physiol Plant 134: 598-608

60. Schwaiger CS, Liin SI, Elinder F, Lindahl E (2013) The Conserved Phenylalanine in the K^+ Channel Voltage-Sensor Domain Creates a Barrier with Unidirectional Effects. Biophysical Journal 104: 75-84

61. Seoh SA, Sigg D, Papazian DM, Bezanilla F (1996) Voltage-sensing residues in the S2 and S4 segments of the Shaker K^+ channel. Neuron 16: 1159-1167

62. Sigworth FJ (2003) Structural biology: Life's transistors. Nature 423: 21-22

63. Silverman WR, Roux B, Papazian DM (2003) Structural basis of two-stage voltage-dependent activation in K^+ channels. Proc Natl Acad Sci USA 100: 2935-2940

64. Spalding EP, Hirsch RE, Lewis DR, Qi Z, Sussman MR, Lewis BD (1999) Potassium uptake supporting plant growth in the absence of AKT1 channel activity - Inhibition by ammonium and stimulation by sodium. J Gen Physiol 113: 909-918

65. Still WC, Tempczyk A, Hawley RC, Hendrikson T (1990) Semianalytical treatment of solvation for molecular mechanics and dynamics. Journal of the American Chemical Society 112: 6127-6129

66. Sutter JU, Campanoni P, Tyrrell M, Blatt MR (2006) Selective mobility and sensitivity to SNAREs is exhibited by the *Arabidopsis* KAT1 K^+ channel at the plasma membrane. Plant Cell 18: 935-954

67. Tao X, Lee A, Limapichat W, Dougherty DA, MacKinnon R (2010) A Gating Charge Transfer Center in Voltage Sensors. Science 328: 67-73

68. Thiel G, Blatt MR (1991) The mechanism of ion permeation through K^+ channels of stomatal guard cells voltage-dependent block by Na^+. J Plant Physiol 138: 326-334

69. Tiwari-Woodruff SK, Lin MCA, Schulteis CT, Papazian DM (2000) Voltage-dependent structural interactions in the Shaker K+ channel. J Gen Physiol 115: 123-138

70. Uozumi N, Gassmann W, Gao YW, Schroeder JI (1995) Identification of strong modifications in cation selectivity in an *Arabidopsis* inward rectifying potassium channel by mutant selection in yeast. J Biol Chem 270: 24276-24281

71. Uozumi N, Nakamura T, Schroeder JI, Muto S (1998) Determination of transmembrane topology of an inward-rectifying potassium channel from Arabidopsis thaliana based on functional expression in Escherichia coli. Proc Natl Acad Sci USA 95: 9773-9778

72. Vargas E, Bezanilla F, Roux B (2011) In Search of a Consensus Model of the Resting State of a Voltage-Sensing Domain. Neuron 72: 713-720

73. Vergani P, Hamilton D, Jarvis S, Blatt MR (1998) Mutations in the pore regions of the yeast K^+ channel YKC1 affect gating by extracellular K^+. EMBO J 17: 7190-7198

74. Very AA, Sentenac H (2003) Molecular mechanisms and regulation of K^+ transport in higher plants. Annual Review of Plant Biology 54: 575-603

75. Wang Y, Hills A, Blatt MR (2014a) Systems analysis of guard cell membrane transport for enhanced stomatal dynamics and water use efficiency. Plant Physiol 164: 1593-1599

76. Wang Y, Papanatsiou M, Eisenach C, Karnik R, Williams M, Hills A, Lew VL, Blatt MR (2012) Systems dynamic modelling of a guard cell Cl^- channel mutant uncovers an

emergent homeostatic network regulating stomatal transpiration. Plant Physiol 160: 1956-1972

77. Wang Y, Noguchi K, Ono N, Inoue Si, Terashima I, Kinoshita T (2014b) Overexpression of plasma membrane H^+-ATPase in guard cells promotes light-induced stomatal opening and enhances plant growth. Proc Nat Acad Sci USA 111: 533-538

78. Yarov-Yarovoy V, Baker D, Catterall WA (2006) Voltage sensor conformations in the open and closed states in ROSETTA structural models of K+ channels. Proceedings Of The National Academy Of Sciences Of The United States Of America 103: 7292-7297

79. Zei PC, Aldrich RW (1998) Voltage-dependent gating of single wild-type and S4 mutant KAT1 inward rectifier potassium channels. J Gen Physiol 112: 679-713

Table 1. Global joint fitting of the voltage-sensor domain mutants of KAT1 expressed in *Xenopus* oocytes. Fittings were to a Boltzmann function of the form

$$I = \frac{g_{max}(V-E_K)}{1+e^{\delta zF(V-V_{1/2})/RT}} \qquad [1]$$

where δ is the voltage sensitivity coefficient (gating charge), E_K is the K^+ equilibrium voltage, g_{max} is the maximum conductance of the ensemble of channels, $V_{1/2}$ the voltage yielding half-maximal activation, and F, R and T have their usual meanings. Fittings were carried out by least-squares error minimization using a Marquardt-Levenberg algorithm (Marquardt 1963) with the combined data sets, allowing a minimum of parameters to vary between data sets. Listed here, and shown in Figs. 2-6, are the results of the best fitting obtained with δ held in common between all data sets and g_{max} held in common between all sets apart from those of the $KAT1^{D105E}$, $KAT1^{D105N}$ and $KAT1^{R177K}$ mutants. Fitted δ, 1.87±0.05

Construct	$V_{1/2}$ (mV)	g_{max} (mS)
$KAT1^{wt}$	-138.9 ±0.6	
$KAT1^{F102W}$	-225.1 ±0.8	
$KAT1^{F102Q}$	-217.0 ±1.1	
$KAT1^{F102S}$	-195.5 ±0.9	83.4 ±0.6
$KAT1^{F102L}$	-157.2 ±0.5	
$KAT1^{D95E}$	-110.3 ±0.8	
$KAT1^{D95N}$	- 78.2 ±0.4	
$KAT1^{D141E}$	-141.2 ±0.9	
$KAT1^{D105E}$	- 90.5 ±1.2	59.1 ±0.5
$KAT1^{D105N}$	- 78.9 ±0.7	51.6 ±0.4

$KAT1^{R177K}$	-	85.1 ±2.1	44.0 ±0.6

Table 2.

Figure Legends:

Fig. 1. Arabidopsis Kv-like channels share a set of highly-conserved acid residues within the S2 and S3 α-helices, and a conserved Phe positioned centrally within the S2 α-helix.
(A) Sequence alignment of several voltage-dependent membrane proteins, KAT1 (GI:15237407), KC1 (KAT3, GI: 15233870), AKT1 (GI:15225768), Kv1.2 (GI:52000923), Nav1.1 (115583677), Cav1.1 (GI:110349767), Hv1 (GI:91992155), VSP(GI:76253898). Conserved residues addressed in this study are color coded: yellow, acidic; green, aromatic.
(B) The KAT1 voltage-sensor domain (VSD) shown in the 'up' (left) and 'down' (right) conformations with phospholipid headgroups (black balls) indicated for reference to the membrane position. The α-helices are color-coded with S1 in front (transparent white), S2 (black), S3 (mauve), S4 (ochre). Also shown are residues (*top to bottom*, blue stick representations) Arg^{165}, Arg^{171}, Arg^{174} and Arg^{177} of the S4 α-helix. Residues Asp^{95}, Asp^{105} and Asp^{141} (acidic, yellow) and Phe^{102} (aromatic, green) are shown in Van der Waals representation.

Fig. 2. Gating of the Arabidopsis KAT1 K^+ channel is displaced negative-going by mutations of Phe^{102}.
(A) Steady-state current-voltage curves for the wild-type channel ($KAT1^{wt}$) and each of four Phe^{102} mutants, $KAT1^{F102W}$, $KAT1^{F102Q}$, $KAT1^{F102S}$, and $KAT1^{F102L}$. Data points are the means ±SE of >7 independent experiments in each case. Solid lines indicate the results of best joint fittings to a Boltzmann function (Eqn. [1]). Fitted parameters are listed in Table 1.
(B) Representative current traces for each $KAT1^{wt}$ and each of the Phe^{102} mutants in (A). Scale: horizontal, 2 s; vertical, 4 μA.
(C) Gating kinetics of the wild-type channel, $KAT1^{wt}$, and each of four Phe^{102} mutants, $KAT1^{F102W}$, $KAT1^{F102Q}$, $KAT1^{F102S}$, and $KAT1^{F102L}$. Shown are the means ±SE of the activation halftimes as a function of clamp voltage (*left*) and deactivation time constants at -50 mV (*right*). Data were from the same data sets as in (A). Solid curves for activation halftimes are empirical fittings to a simple exponential function with offset and are included for visual guidance only.

Fig. 3. The KAT1 voltage-sensor domain (VSD) forms a stable, hydrophobic pocket to the outside of the Phe^{102} residue.

(A) The VSD shown in the 'up' (left) and 'down' (right) conformations with phospholipid headgroups (black balls) indicated for reference to the membrane position. The α-helices are color-coded with S1 in front (transparent white), S2 (black), S3 (mauve), S4 (ochre). Also shown are residues (*top to bottom*, blue stick representations) Arg^{165}, Arg^{171}, Arg^{174} and Arg^{177} of the S4 α-helix. Residues Asp^{95}, Asp^{105} and Asp^{141} (acidic, yellow) and Phe^{102} (aromatic, green) are shown in Van der Waals representation. The water surface within 10 Å of all of these residues is shown in aquamarine.

(B) Change in the ratio of hydrophobic/hydrophillic surface (Lins et al. 2003) for each of four Phe^{102} mutants, $KAT1^{F102W}$, $KAT1^{F102Q}$, $KAT1^{F102S}$, $KAT1^{F102L}$ and for $KAT1^{wt}$ relative to $KAT1^{wt}$.

Fig. 4. Gating of the Arabidopsis KAT1 K^+ channel is displaced positive-going by mutations of the S2 α-helix residue Asp^{95}.

(A) Steady-state current-voltage curves for the wild-type channel ($KAT1^{wt}$) and the mutants, $KAT1^{D95E}$ and $KAT1^{D95N}$. Data points are the means ±SE of >6 independent experiments in each case. Solid lines indicate the results of best joint fittings to a Boltzmann function (Eqn. [1]). Fitted parameters are listed in Table 1. *Insets*: Representative current traces for $KAT1^{wt}$ and the $KAT1^{D95E}$ mutant. Scale: horizontal, 2 s; vertical, 4 μA.

(B) Gating kinetics of the wild-type channel, $KAT1^{wt}$, and the mutants, $KAT1^{D95E}$ and $KAT1^{D95N}$. Shown are the means ±SE of the activation halftimes as a function of clamp voltage (*left*) and deactivation time constants at -50 mV (*right*). Data were from the same data sets as in (A). Solid curves for activation halftimes are empirical fittings to a simple exponential function with offset and are included for visual guidance only.

(C) The S2 (black) and S4 (ochre) α-helices of the VSD shown in the 'up' (left) and 'down' (right) conformation. Residues (*top to bottom*, blue) Arg^{165}, Arg^{171}, Arg^{174} and Arg^{177} of the S4 α-helix and residue Asp^{95} (red) are shown in stick representation. Critical distances of the terminal residue carbons are indicated by the dotted lines. Asp^{95} is predicted to interact with Arg^{171} and Arg^{174} in the 'up' state, and with Arg^{165} in the 'down' state. Distances resolved following molecular-dynamic equilibration are listed in Table 2.

Fig. 5. Gating of the Arabidopsis KAT1 K^+ channel is displaced positive-going by mutations of the S2 and S4 α-helix residues Asp^{105} and Arg^{177}, but not by Asp^{141}.

(A) Steady-state current-voltage curves for the wild-type channel ($KAT1^{wt}$) and the mutants, $KAT1^{D105E}$, $KAT1^{D105N}$, $KAT1^{D141E}$ and $KAT1^{R177K}$. Data points are the means ±SE of >7 independent experiments in each case. Solid lines indicate the results of best joint fittings to a Boltzmann function (Eqn. [1]). Fitted parameters are listed in Table 1. *Insets*: Representative current traces for $KAT1^{wt}$ and the $KAT1^{D95E}$, $KAT1^{D105E}$, $KAT1^{D141E}$, and $KAT1^{R177K}$ mutants. Scale: horizontal, 2 s; vertical, 4 μA.

(B) Gating kinetics of the wild-type channel, $KAT1^{wt}$, and each of the mutants $KAT1^{D105E}$, $KAT1^{D105N}$, $KAT1^{D141E}$ and $KAT1^{R177K}$. Shown are the means ±SE of the activation halftimes as a function of clamp voltage (*left*) and deactivation time constants at -50 mV (*right*). Data were from the same data sets as in (A). Solid curves for activation halftimes are empirical fittings to a simple exponential function with offset and are included for visual guidance only.

(C) The S2 (black), S3 (mauve), and S4 (ochre) α-helices of the VSD shown in the 'up' (left) and 'down' (right) conformation. Residues (*top to bottom*, blue) Arg^{165}, Arg^{171}, Arg^{174} and Arg^{177} of the S4 α-helix and residues Asp^{105} and Asp^{141} (red) are shown in stick representation. Critical distances of the terminal residue carbons are indicated by the dotted lines. Asp^{105} is predicted to interact weakly with Arg^{171} in the 'down' state; Asp^{141} is predicted to interact in the 'up' state with Arg^{177} and in the 'down' state with Arg^{171}. Distances resolved following molecular-dynamic equilibration are listed in Table 2.

Fig. 6. Reaction kinetic analysis of gating for KAT1 and the several mutations studied. Fittings were carried out by least-squares minimization to a three-state model (see **RESULTS**) using a Marquardt-Levenberg algorithm (Marquardt 1963). Best fittings were obtained with the following parameters fixed between all data sets: k_{32}^{o}, $6.1\times10^{-6} \pm 1.2\times10^{-6}$ s^{-1}; k_{23}^{o}, $1.8\times10^{-6} \pm 0.6\times10^{-6}$ s^{-1}; δ_{32}, -1.86±0.06 e^-; δ_{21}, -0.95±0.01 e^-; δ_{12}, 0.48±0.01 e^-. δ_{23} in all trials yielded values of less than 0.0002 and was therefore fixed to zero. Parameters for k_{21}^{o} and k_{12}^{o} varied between mutations of Phe^{102} and parameters for k_{21}^{o} alone varied for

mutations of Asp^{95}, Asp^{105}, Asp^{141} and Arg^{177}. Values for these parameters are summarized in Fig. 7.

(A) Steady-state conductance-voltage data sets derived from the current-voltage curves in Figs. 2, 4 and 5 and fitted to Eqn. 6 (solid lines).

(B) Activation and deactivation kinetics for selected mutations. Data sets for all mutations, including those shown, were fitted to Eqn. 4 (solid lines) after thinning the data point density as shown for ease of handling. Scale: 5 μA vertical, 1 s horizontal (activation); 2.5 μA vertical, 0.3 s horizontal (deactivation).

Fig. 7. Variable parameter values from the reaction kinetic analysis of gating for KAT1 and the several mutations studied. Parameter values are for k_{21}^{o} and k_{12}^{o} which varied between mutations of Phe^{102}, and for k_{21}^{o} which alone varied for mutations of Asp^{95}, Asp^{105}, Asp^{141} and Arg^{177}. Note the logarithmic scale for both k_{21}^{o} and k_{12}^{o}.

Table 2. Terminal C-C carbon atom distances from residue sites and mutations to critical charged residues (indicated). Distances determined during 10 ns equilibration (See Suppl. Fig. S1) are reported for the two states of the voltage-sensor domain. Values without standard errors represent distances in the absence of key residue interactions and, hence, were not pursued further. Values in bold highlight dominant spacings affecting charge interactions. Shading favoring the open channel (blue) and closed channel (red). Absolute electrostatic (Elec) and solvation energies (Sol) in kJ/mol of the OPLS force field calculated for the key residue interactions as indicated (Alves, et al. 2007). The generalized Born energy for solvation was calculated according to Still, et al. (1990). Note that using C-C distances adds 1 Å to the maximum for salt formation.

Site	Mutation		Down (open) state				Up (closed) state			
		Residue	Distance (Å)	salt bridge?	Elec (kJ/mol)	Sol (kJ/mol)	Distance (Å)	salt bridge?	Elec (kJ/mol)	Sol (kJ/mol)
D95	WT	R165	**4.48±0.08**	Y	-284±6	274±5	20.47±1.31			
		R171	14.89±0.08				**4.43±0.06**	Y	-368±13	314±6
		R174	20.75±0.83				**4.62±0.06**	Y	-388±13	313±6
		R177	24.92±0.76				9.35±0.07			
	D95E	R165	**4.84±0.16**	Y	-453±14	354±8	19.52±1.11			
		R171	15.08±1.72				**6.02±0.06**	N	-367±11	306±5
		R174	21.44±1.23				**5.06±0.06**	N	-403±12	328±6
		R177	26.08±1.93				12.91±1.79			
	D95N	R165	**4.40±0.06**	N	-59±6	29±4	19.51±1.39			
		R171	15.07±0.71				**6.06±0.06**	N	-1±3	0±3
		R174	21.14±1.23				**5.26±0.06**	N	-72±4	60±3
		R177	25.25±1.28				10.56±0.64			
D105	WT	R165	15.16±0.07				32.9±1.4			
		R171	**10.92±0.06**	N	-100±1	99±1	21.3±0.7			
		R174	17.96±1.07				15.7±0.7			
		R177	25.78±0.95				11.6±0.6			
	D105E	R165	18.66±1.05				33.88			
		R171	**7.99±0.06**	N	-244±3	239±3	24.19			
		R174	16.10±1.46				15.83			
		R177	23.68±0.90				11.61			
	D105N	R165	17.67±0.99				33.36			
		R171	**6.13±0.57**	N	2±11	-2±11	22.84			
		R174	14.34±0.82				14.48			
		R177	22.54±1.20				10.24			
D141	WT	R165	**10.95±0.07**				23,8±1,36			
		R171	**3.95±0.05**	Y	-506±14	381±5	13,4±0,07			
		R174	11.97±0.93				**8,15±0,07**			
		R177	19.45±0.92				**3,53±0,07**	Y	-389±12	354±6
	D141E	R165	**13.24±1.01**				25,5±1,46			
		R171	**5.27±0.06**	N	-374±10	314±5	14,11±0,51			
		R174	14.57±1.42				**10,04±0,35**			
		R177	19.34±0.87				**5,28±0,06**	N	-473±14	383±6
R177	WT	D95	25.29±0.34				9.01±0.08			
		D105	26.42±0.44				11.51±0.11			
		D141	20.07±0.46				**4.13±0.04**	Y	-389±13	354±6
	R177K	D95	27.39				8.85±0.09			
		D105	25.67				11.27±0.13			
		D141	19.91				**4.81±0.07**	Y	-332±10	287±5

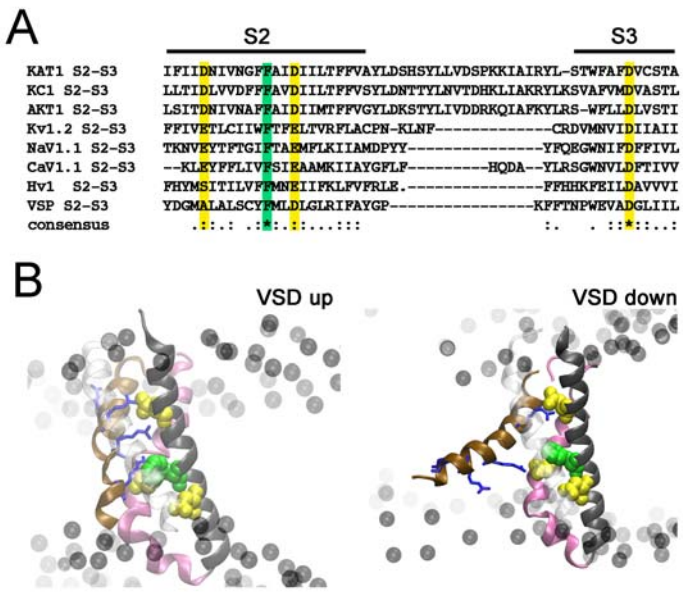

Fig. 1

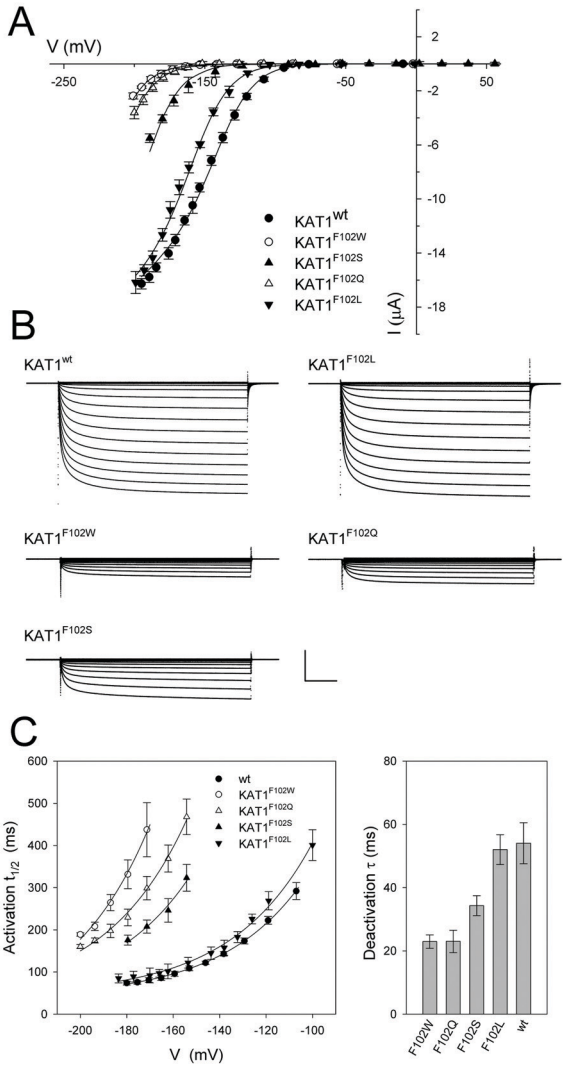

Fig. 2

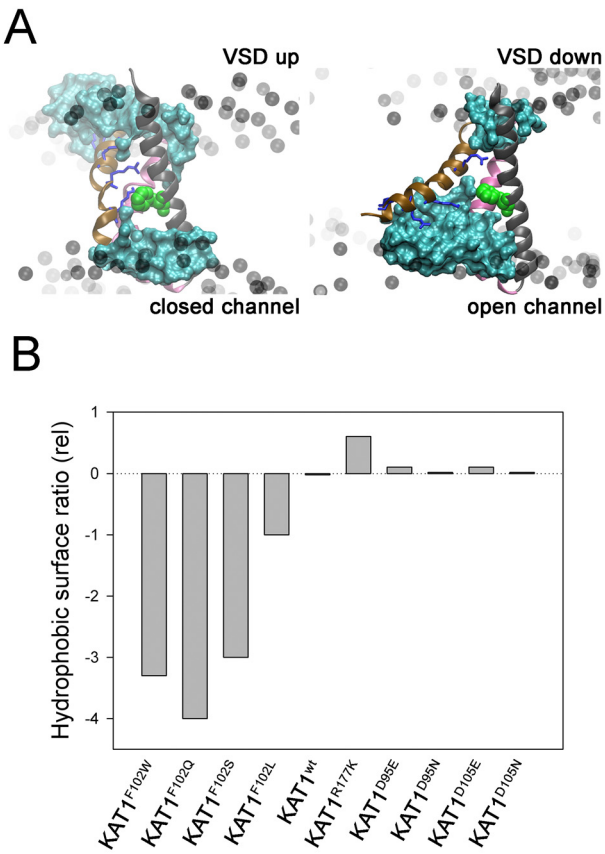

Fig. 3

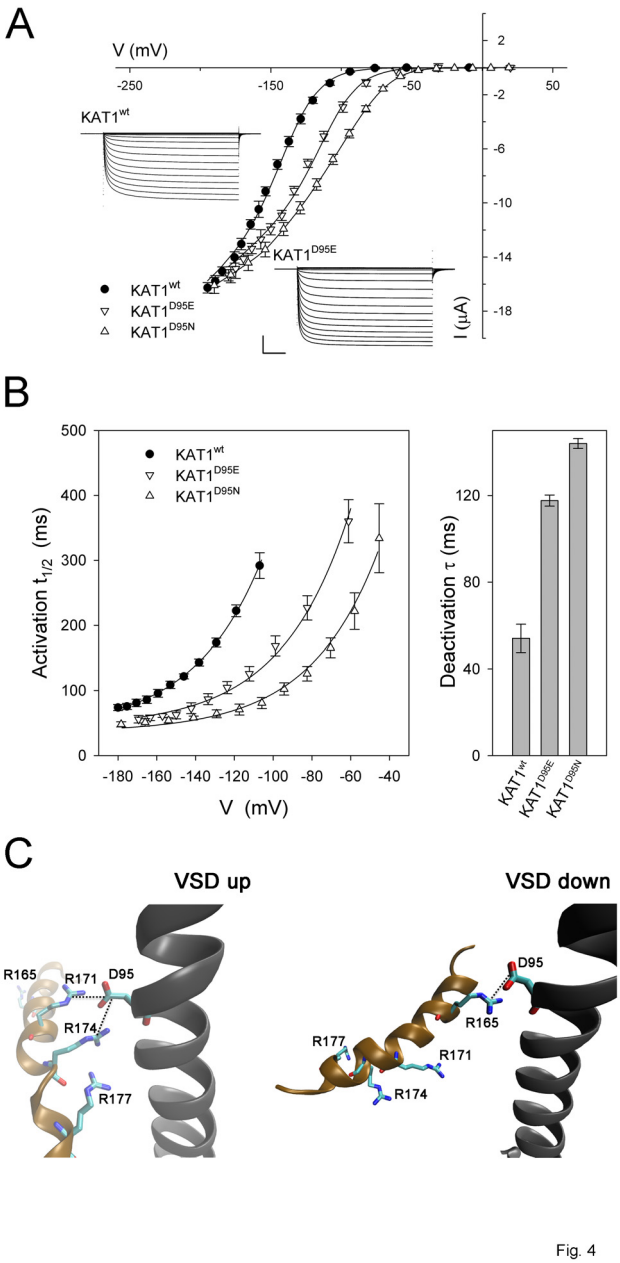

Fig. 4

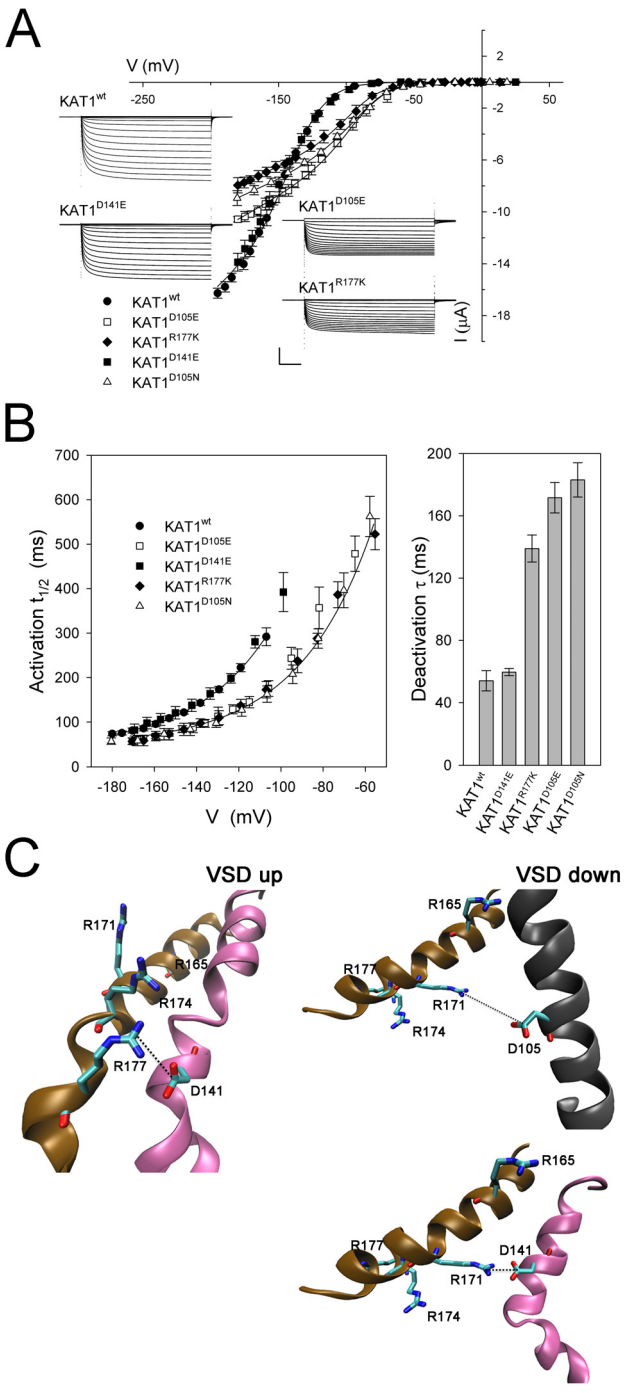

Fig. 5

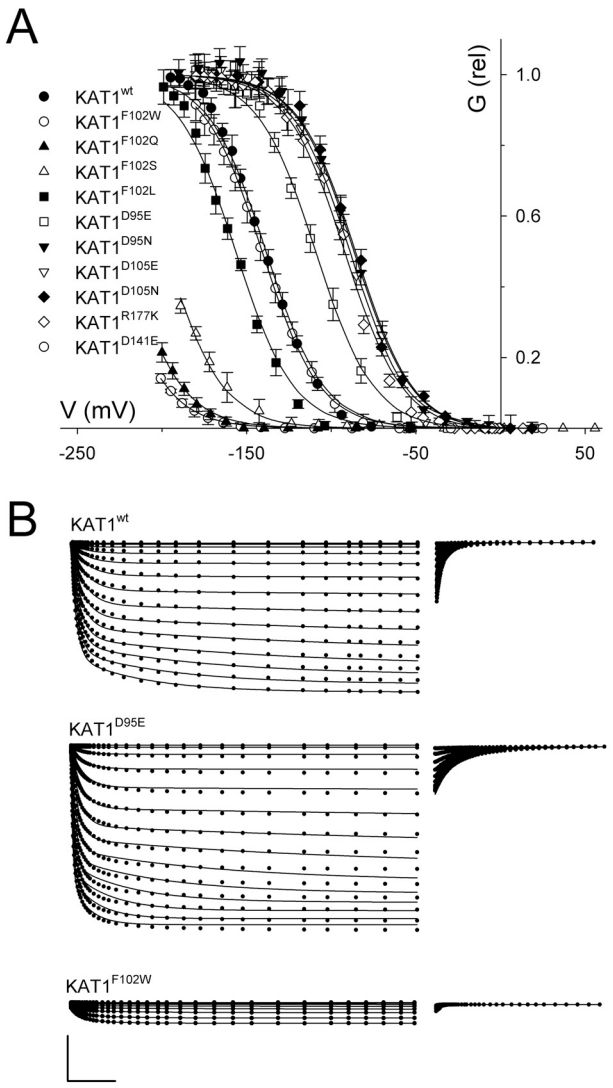

Fig. 6

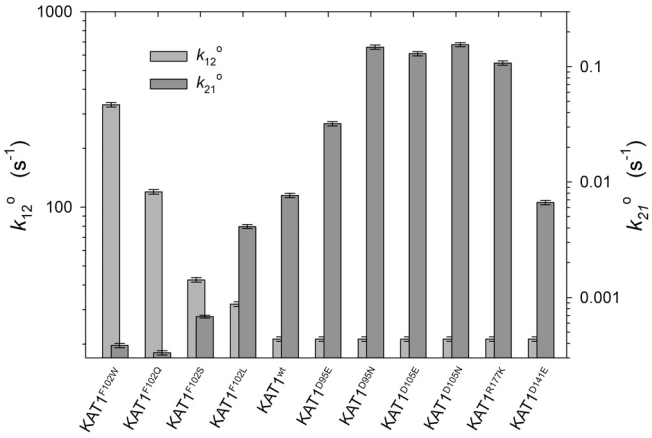

Fig. 7